Available online at www.sciencedirect.com
ScienceDirect
Polymer 48 (2007) 2371–2379
polymer
www.elsevier.com/locate/polymer

Stress prediction for polymer blends with various shapes of droplet phase

Masaoki Takahashi*, Paulo H.P. Macaúbas[1], Kenzo Okamoto, Hiroshi Jinnai, Yukihiro Nishikawa

Department of Macromolecular Science and Engineering, Kyoto Institute of Technology, Matsugasaki, Sakyo-Ku, Kyoto 606-8585, Japan

Received 26 September 2006; received in revised form 18 February 2007; accepted 25 February 2007
Available online 28 February 2007

Abstract

The excess shear stress after application of large step strains in polymer blend is calculated from observed shapes of deformed droplets in immiscible matrix, based on the Doi–Ohta expression for the interface contribution to the stress. The calculation is made for droplet shapes of flat ellipsoid, rod with end caps, dumbbell and ellipsoid of revolution. The predicted excess relaxation modulus agrees very well with experimental data normalized per one droplet with the volume-averaged radius for a poly(isobutylene)/poly(dimethyl siloxane) blend with narrow distribution of droplet size. Especially, slow stress relaxation in the intermediate stage and faster relaxation thereafter predicted from the rod like and dumbbell shapes are consistent with the experimental data. For a blend of hydroxypropylcellulose solution/poly(dimethyl siloxane) with broad distribution of droplet size, the predicted excess relaxation modulus agrees reasonably well with experimental data by taking account of the size distribution.

Keywords: Polymer blend; Interface tensor; Droplet phase

1. Introduction

Stress prediction for immiscible polymer blends under flow has long been investigated. From an industrial point of view, the stress prediction is important for finding better process condition and for controlling blend morphology. However, the stress prediction is still very difficult, because the excess stress due to the anisotropy of interface is directly related to evolution of interface shape under flow. A variety of models has been presented to describe micro structural evolution and associated rheology [1]. Ellipsoidal and rod-like models have been typical examples for the deformed droplet shapes. Experimentally, however, there appear dumbbell shape and stretched thread with bulbous ends in relaxation process due to the end-pinching, Rayleigh instability and pressure gradient inside the droplet [2] in much wider range of viscosity ratio than generally expected. The viscosity ratio K and interfacial tension govern the shape of deformed droplet phase and the interfacial stress. Here, K is defined by $K = \eta_d/\eta_m$, where subscripts d and m denote droplet and matrix, respectively. Systematic experimental studies on stretched droplet shapes after cessation of planar extensional flows revealed that the dumbbell shape appeared in blends of Newtonian fluids in very wide range of K, such as $0.01 \leq K \leq 11$ [3].

For immiscible binary blends, a basic equation relating the interface shape and the volume-averaged excess stress tensor $\mathbf{\Delta\sigma}$ was presented by Batchelor [4] and cast in the following form by Onuki [5,6] and Doi and Ohta [7] as

$$\mathbf{\Delta\sigma} = -\Gamma\mathbf{q} = -\frac{\Gamma}{V}\int \mathrm{d}S\left(\mathbf{nn} - \frac{1}{3}\mathbf{I}\right) \tag{1}$$

In Eq. (1), Γ is the interfacial tension and $\mathbf{q}$ is the interface tensor. V represents the entire volume of the system, $\mathbf{nn}$ is the dyadic of the unit vector $\mathbf{n}$ normal to the interface, and $\mathbf{I}$ denotes the unit tensor. The integration is made over the entire interface of the system. The tensor $\mathbf{q}$ represents the anisotropy of

* Corresponding author. Tel.: +81 75 724 7835; fax: +81 75 724 7800.
E-mail address: mdt@kit.ac.jp (M. Takahashi).
[1] On leave from Department of Metallurgical and Materials Engineering, Escola Politécnica, São Paulo University, Av. Prof. Mello Moraes, 2463, CEP 05508-900, São Paulo, SP, Brazil.

0032-3861/$ - see front matter © 2007 Elsevier Ltd. All rights reserved.
doi:10.1016/j.polymer.2007.02.056

the interface due to flow and determines the interface stress. This expression is first proposed for dilute blends [4] but can be used for concentrated blends as well [5–7]. It should be noted here that in general, another term concerning the velocity field at the interface and the viscosity difference between the components should be added [4,6]. This term may be ignored for systems of equal viscosity [7]. An anonymous reviewer pointed out the importance of local flow of the medium around a droplet in the recovery process where shrinkage in the direction of the major axis and expansion along the minor axes cause negative and positive pressures and the matrix near the minor axis flows in the direction of the major axis. We thank the reviewer for the kind suggestion on this important problem. At the present state, we do not know how to incorporate this problem and to evaluate the term concerning the velocity at the interface. Thus, only the term concerning the interface shape is evaluated in the present study. In that case, once the shape of interface in the deformed state can be obtained, Eq. (1) is extremely useful for calculating the interface contribution to the stress. However, direct evaluation of Eq. (1) using experimental data has not been made concerning shapes other than ellipsoidal, such as dumbbell and rod-like shapes.

The objectives of the present study are (1) experimental evaluation of the basic Eq. (1) in two blend systems with very different K and Γ, and (2) proposal for stress calculation method in polydisperse droplet systems. In the present study, evaluations are made for relaxation process after application of large step shear strains. In the step-strain experiment, droplet deformation and relaxation can be determined unambiguously, when neither breakup nor coalescence occurs. A retraction time of the major axis of a deformed droplet is much shorter than the rotational relaxation time. The very slow orientation relaxation results in a constant orientation angle during the stress relaxation [8–10]. We can expect neither breakup nor coalescence of droplets under certain conditions of the droplet fraction (lower than ca. 20 vol%) and the external step shear strain (smaller than ca. 5) in wide range of K and Γ.

As shown by Yamane *et al.* [8], the droplet shape observed at large step strains could be classified as flat ellipsoid, rod-like shape, dumbbell and ellipsoid of revolution as schematically shown in Fig. 1. The droplet shape changes in this order to reduce the interfacial free energy [9]. It should be emphasized here that the characteristic length scale is not determined by the external field in step-strain experiments without breakup. Even if we apply the Doi–Ohta simultaneous equations [7] for the specific interface area, Q, and the normalized interface tensor, $\mathbf{q}/Q$, the predicted relaxation stress is inconsistent with experimental data as shown by Okamoto *et al.* [11]. However, we can still use the basic Eq. (1), which is free from this limitation.

In preliminary investigations on poly(isobutylene) (PIB)/poly(dimethyl siloxane) (PDMS) system with $K = 0.067$, 1.1, 4.5, 11 and 15, we have observed the dumbbell shape for $K \leq 4.5$ at the strain of $\gamma = 5$ and/or 7. In the present study, stress calculation and comparison with experimental data will be made on a PIB/PDMS system with $K = 0.067$ and on a hydroxypropylcellulose (HPC) solution/PDMS system with $K = 0.54$. This isotropic HPC solution/PDMS system has higher Γ and much broader distribution of droplet size than those of PIB/PDMS system, and is an interesting system to investigate the applicability of Eq. (1).

Recently, Almusallam *et al.* [12] proposed a comprehensive constitutive equation incorporating the convection, retraction, breakup and coalescence of droplets for immiscible Newtonian blends. Adopting an ellipsoidal model, Maffettone and Greco [13] treated the deformation of a viscoelastic droplet in a viscoelastic matrix. They predict that the matrix elasticity clearly retards the droplet relaxation. Further, Yu *et al.* [14] treated the viscoelastic droplet deformation and also concluded that the matrix elasticity slows down the relaxation. In the present study, we will consider systems where the elastic effects can be neglected and the droplet relaxation can be described by η_m, K, Γ and the equilibrium radius r_0. It is the purpose of this paper to investigate Eq. (1) in most simplified and unambiguous way.

2. Calculation of the excess shear stress from the deformed droplet shape

In order to compare theoretical predictions for a single droplet with data of a real polydisperse droplet system, we define the volume fraction ϕ for a single droplet with the radius r_0 by $\phi = (4\pi r_0^3/3)(n/V)$ with $n = 1$. From Eq. (1), the excess shear stress $\Delta\sigma_{xy}$ can be written as

$$\Delta\sigma_{xy} = -\frac{3\Gamma\phi}{4\pi r_0^3}\int \mathrm{d}S\, n_x n_y \tag{2}$$

where x and y are flow and flow-gradient directions. In Fig. 2, the semi-major (a) and semi-minor axes (b and c) for ellipsoid, rod-like shape and dumbbell are schematically shown together with the orientation angle θ to the flow direction x. In case of

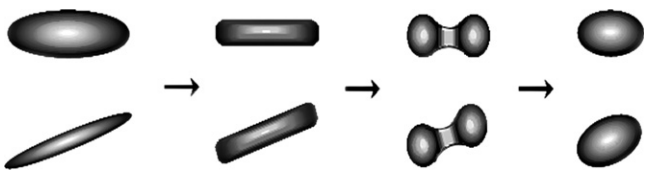

Fig. 1. Change in the droplet shape after application of a large step shear strain: Top view (upper) and side view (lower).

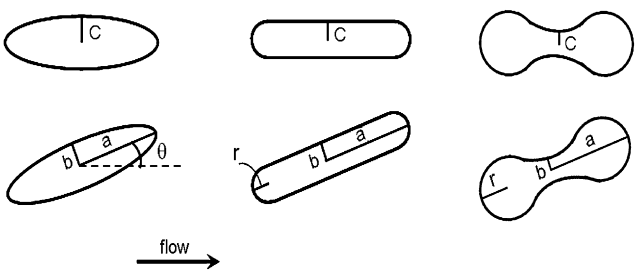

Fig. 2. Definition of semi-axes, orientation angle and radius of semi-sphere of end caps: Top view (upper) and side view (lower).

dumbbell, b and c denote midsection radius. Experimentally, the dumbbell shape can be fitted with a surface of rotated cosine curve, end-capped with hemi-spheres of radius r ($>b=c$) [9]. For each droplet shape, an analytical solution of Eq. (2) (or an integral equation for numerical calculation) is derived and summarized in Table 1. The volume conservation requirement is applied to all the droplet shapes.

When the orientation angle θ of a droplet is equal to an angle given by affine deformation assumption, θ satisfies the following equation

$$\cot 2\theta = \gamma/2 \tag{3}$$

where γ is the external step strain applied. The affine deformation assumption is a reasonable one for droplets with $K=1$ [15], because initial stretch is also close to the affine deformed value when $K=1$. Experimentally, Eq. (3) holds for droplets with $K=0.067$ [8–10] and $K=0.0476$ [11] all through the relaxation process, probably because the initial principal stretch a/r_0 exceeds the affine-deformed value only slightly (25%) even at very small $K=0.067$. In the preliminary investigation, Eq. (3) also holds for $K=1.1$, while systematic deviation from this angle to lower one (excessive rotation) is observed for $K\geq 4.5$. In the present study, $K=0.067$ and $K=0.54$, and thus Eq. (3) is used in the stress calculation.

3. Experimental

3.1. Samples

Two blend systems, PIB/PDMS and HPC25%/PDMS, are used in the present study. Rheological parameters, η_m, K and Γ, measured at 23 °C are summarized in Table 2. The weight-average molecular weights of PIB and HPC are 1.35×10^3 and 1.0×10^5, respectively. HPC25% is a 25 wt% solution in water, and the solution is in the isotropic state. As shown in Table 2, PDMS of different viscosity is used as a matrix in each blend. The values of Γ were obtained by applying the pendant drop method [16] and the short fiber retraction method with some improvement [17]. A 20/80 (wt/wt) blend of each system is prepared. To obtain reproducible distribution of droplet size, pre-shear was given before all the stress relaxation measurements. A very small amount of fluorescein sodium salt (0.02 wt%) was added to HPC25% component to detect the distribution of droplet size. It was confirmed that the interfacial tension did not change by this addition.

3.2. Apparatuses

Observation of deformed PIB droplets in the PDMS matrix using a sliding-plate apparatus is already described in the previous papers [8,9]. The same sliding-plate apparatus with enhanced gap of 2.7 mm was utilized to observe HPC25% droplets in other PDMS matrix. For the 20/80 blends of both systems, a new rheo-optical apparatus of rotational type, RheoOptica 1 (UBM Co. Ltd. in Japan) equipped with an optical microscope or a polarized optical microscope was used to detect the distribution of equilibrium droplet size after pre-shear. For both blends, stress relaxation data were obtained with ARES (Rheometric Scientific) using a cone-plate geometry with 25 mm diameter and 0.1 rad gap angle. A parallel-plate geometry with 50 mm diameter and 1 mm gap was also utilized to cover low stress data. The Soskey–Winter correction [18] for non-uniform strain was made for the parallel-plate data. To confirm accuracy of the relaxation data, Gemini (Malvern Instruments) was also used with a cone-plate geometry of 40 mm diameter and 4° gap angle. In the present study, only the stress relaxation data are shown in the range where ARES and Gemini give identical result. Dynamic viscoelastic measurements were made using ARES with the same cone-plate and parallel-plate geometries.

Table 1
The excess shear stress calculated based on Eq. (2)

Shape	Excess shear stress
Ellipsoid ($a\geq c\geq b$)	$\Delta\sigma_{xy}=-\left(\frac{3\Gamma\phi}{8\pi r_0}\right)\sin 2\theta\int_0^{2\pi}\mathrm{d}\Phi\int_0^{\pi}\mathrm{d}\Theta\sin\Theta\frac{\frac{\cos^2\Theta}{\lambda_1^2}-\frac{\sin^2\Theta\cos^2\Phi}{\lambda_2^2}}{\sqrt{\frac{\cos^2\Theta}{\lambda_1^2}+\left(\frac{\cos^2\Phi}{\lambda_2^2}+\frac{\sin^2\Phi}{\lambda_3^2}\right)\sin^2\Theta}}$, $\lambda_1=a/r_0$, $\lambda_2=b/r_0$, $\lambda_3=c/r_0$ with $\lambda_1\lambda_2\lambda_3=1$
Rod-like shape	$\Delta\sigma_{xy}=\left(\frac{3\Gamma\phi}{8r_0}\right)\sin 2\theta[2(\lambda-R)R]$, $\lambda=a/r_0$, $R=b/r_0=c/r_0=r/r_0$
Dumbbell	$\Delta\sigma_{xy}=-\left(\frac{3\Gamma\phi}{8r_0}\right)\sin 2\theta\int_{-(\lambda_1-R)}^{\lambda_1-R}\mathrm{d}X\left[\frac{\lambda_2-R}{2}\cos\left(\frac{\pi X}{\lambda_1-R}\right)+\frac{\lambda_2+R}{2}\right]\times\left[\frac{\pi^2}{4}\left(\frac{\lambda_2-R}{\lambda_1-R}\right)^2\sin^2\left(\frac{\pi X}{\lambda_1-R}\right)+1\right]^{-1/2}\left[\frac{\pi^2}{2}\left(\frac{\lambda_2-R}{\lambda_1-R}\right)^2\sin^2\left(\frac{\pi X}{\lambda_1-R}\right)-1\right]$
	$\lambda_1=a/r_0$, $\lambda_2=b/r_0=c/r_0$, $R=r/r_0$, $X=\xi/r_0$. ξ: coordinate axis parallel to the major axis
Ellipsoid of revolution	$\Delta\sigma_{xy}=\left(\frac{3\Gamma\phi}{8r_0}\right)\sin 2\theta\left[\frac{\lambda^3+2}{\lambda(\lambda^3-1)}+\frac{\sqrt{\lambda}(\lambda^3-4)}{(\lambda^3-1)}\frac{\arcsin\sqrt{1-\lambda^{-3}}}{\sqrt{1-\lambda^{-3}}}\right]$, $\lambda=a/r_0$, $b/r_0=c/r_0=\lambda^{-1/2}$

Table 2
Characteristics of 20/80 blends measured at 23 °C

Sample	η_m (Pa s)	K	Γ (N/m)	r_V (μm)	ϕ	τ_D (s)
PIB/PDMS	900	0.067	3.1×10^{-3}	9.0	0.214	4.1
HPC25%/PDMS	270	0.54	8.4×10^{-3}	14.7	0.186	0.97

4. Results and discussion

4.1. Droplet dimensions and calculated modulus for a single droplet

Fig. 3 (upper) shows time dependences of normalized semi-axes a/r_0, b/r_0 and c/r_0, at $\gamma = 5$. Open symbols denote PIB(droplet)/PDMS data for $r_0 = 230$ μm reproduced from the previous study [8], while closed symbols represent data for HPC25%(droplet)/PDMS system with $r_0 = 220$ μm. The time t is normalized by τ_D, a linear viscoelastic relaxation time of Palierne [19] with $\phi \to 0$

$$\tau_D = \frac{\eta_m r_0}{\Gamma} \frac{(19K+16)(2K+3)}{40(K+1)} \tag{4}$$

The time τ_D is 84.7 s for PIB droplet and 12.3 s for HPC25% droplet. In Fig. 3, the vertical solid lines for PIB droplet and broken lines for HPC25% droplet are drawn to show each period of shape changing process. It was found in the PIB/PDMS system that the plots of normalized semi-axes vs. normalized time for droplets with r_0 in the range of 140–280 μm coincide at each γ [9]. This means that in this normalized plots the shape recovery process including several shape transitions does not depend on the droplet size in the measured range of droplet size. All characteristic times for shape recovery may be proportional to r_0, because τ_D is proportional to r_0. For the HPC25%/PDMS system, the droplet-size independence has been observed in the present study in the range of 97–252 μm.

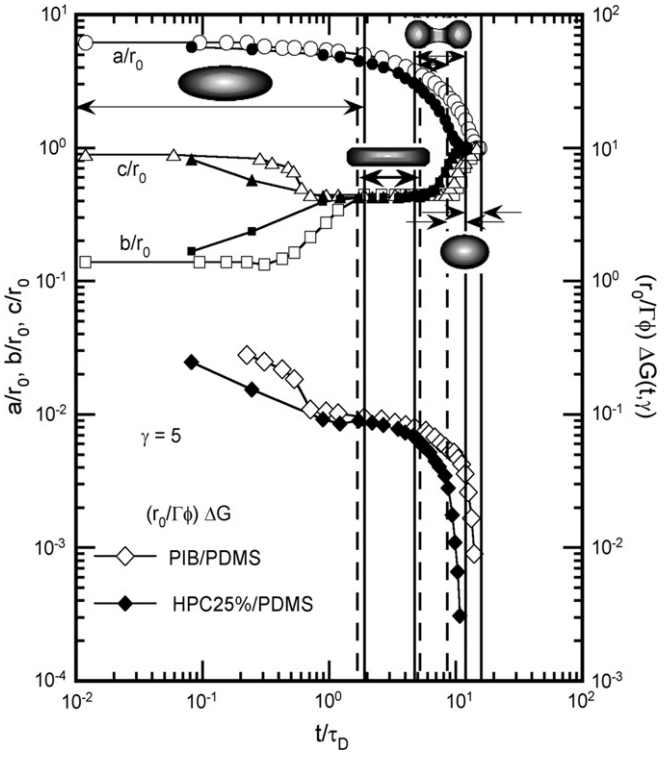

Fig. 3. Time dependences of semi-major and semi-minor axes of a single droplet (upper) and calculated excess relaxation modulus (lower). Open and closed symbols denote data for a PIB droplet ($r_0 = 230$ μm) and a HPC25% droplet ($r_0 = 220$ μm) in each PDMS matrix.

Here we consider the appearance of dumbbell shape or cause of non-existence of multi-constrictions in the measured region of γ. An anonymous reviewer suggested estimation of the wavelength of the Rayleigh instability. We thank the reviewer for the pertinent suggestion. The wavelength λ_M of the Rayleigh instability was estimated using the Tomotika theory [20] with an approximation of infinite length for a cylindrical droplet. The maximum growth rate q_M of the Rayleigh wave for an infinitely long thread is given by

$$q_M = \frac{\Gamma \Omega(\lambda_M, K)}{2\eta_m r_{ini}} \tag{5}$$

where λ_M and r_{ini} are the dominant wavelength of distortion and the initial thread radius, and $\Omega(\lambda,K)$ denotes the Tomotika function [20]. For a given K, Ω becomes a function of normalized wave number $X = kr_{ini} = 2\pi r_{ini}/\lambda$, and has a maximum $\Omega_M = \Omega(\lambda_M,K)$. The corresponding dominant wave number X_M and wavelength λ_M can be determined, where $r_{ini} = b = c$ at the time when a droplet becomes the rod-like shape. For the PIB/PDMS system ($r_0 = 230$ μm), λ_M becomes $6.2r_0$, $4.8r_0$ and $4.2r_0$ at $\gamma = 3$, 4 and 5, while $2a$ is $4.9r_0$, $7.8r_0$ and $10r_0$ at the same strain. Similarly for the HPC25%/PDMS system ($r_0 = 220$ μm), λ_M is calculated to be $6.0r_0$ and $4.2r_0$ at $\gamma = 3$ and 5, while $2a$ is $4.7r_0$ and $9.0r_0$. Comparing λ_M with $2a$, the wavelength is longer than the major axis at $\gamma = 3$, and there may be no possibility for multi-constrictions. However, at larger strains the wavelength becomes smaller than the major axis. Especially, at $\gamma = 5$ the wavelength is roughly 1/2 of the major axis. Thus it is necessary to calculate the amplitude A of the dominant wave in the rod-like period.

$$A = A_0 \exp[q_M(t - t_0)] \tag{6}$$

Here, A_0 is the initial thermal fluctuation and t_0 is the time when the droplet becomes the rod-like shape. Based on the Kuhn theory, Elemans *et al*. evaluated A_0 by

$$A_0 = \left(\frac{21 k_B T}{8\pi^{3/2}\Gamma}\right)^{1/2} \tag{7}$$

where k_B is the Boltzmann constant and T is the absolute temperature [21]. The calculated initial thermal fluctuation is smaller than 1 nm, and the amplitude at the end of the rod-like period becomes negligibly small (1.8 nm for PIB/PDMS and 0.8 nm for HPC/PDMS systems at $\gamma = 5$). The small amplitude is due to large η_m and r_{ini} (or small q_M) and to a relatively short period of time with the rod-like shape. The end-pinching mechanism is considered to be the main cause of appearance of the dumbbell shape at $\gamma \leq 5$.

In Fig. 3 (lower), normalized excess relaxation moduli of the two systems are shown, which are calculated based on the results listed in Table 1. Here, we define the excess relaxation modulus by $\Delta G(t,\gamma) = \Delta\sigma_{xy}/\gamma$, and represent it in a normalized form, $(r_0/\Gamma\phi)\Delta G(t,\gamma)$. Considering a possible experimental error in the smallest semi-axis, b/r_0, we used only the data

of a/r_0 and c/r_0 in the calculation. The value of b/r_0 is estimated based on the constant volume condition. The fast relaxation at short times in the calculated modulus corresponds to the shape change into axial symmetry, and the subsequent plateau region reflects small change in dimension in the rod-like stage. The modulus decays continuously in the dumbbell stage, and then decreases rapidly in the terminal region reflecting the change from ellipsoid of revolution to sphere. It seems that the calculated modulus for the PIB/PDMS system in Fig. 3 relaxes faster than a single exponential decay in both the short time and terminal regions. However, when the modulus is plotted semi-logarithmically against time, a straight line is obtained in each region (first five plots in the flat-ellipsoid stage and last four plots in the ellipsoid-of-revolution stage). From the slope, we can see that the relaxation time is close to τ_D in the terminal region, and the time is about $0.3\tau_D$ in the short time region. It should be noted here that if we include dumbbell or rod-dumbbell stage in addition to the ellipsoid-of-revolution stage, the modulus cannot be expressed by a single exponential decay.

4.2. Distribution of droplet size in the 20/80 blend

Before rheological measurements, the pre-shear at the shear rate of $\dot{\gamma} = 0.25\ s^{-1}$ for 1240 s was given to the PIB/PDMS blend, while $0.5\ s^{-1}$ pre-shear for 1500 s was given to the HPC25%/PDMS blend. In the PIB/PDMS blend, it is very difficult to determine the distribution of droplet size. After the pre-shear and also at rest, the 20/80 blend of PIB/PDMS is in a white creamy state. Since fluorescein is hydrophilic, it cannot be used in a hydrophobic system like a PIB/PDMS blend. The volume-averaged radius $r_V = 9.0$ μm of this blend is evaluated from a comparison between dynamic viscoelastic data and prediction of the emulsion model by Palierne [19]. However, from direct observation using a new apparatus RheoOptica 1, it was found that the number-averaged radius r_N is around 8 μm and that the distribution is rather narrow ($r_V/r_N < 1.2$). On the other hand, the distribution of droplet size in the 20/80 blend of HPC25%/PDMS with fluorescein sodium salt was determined after pre-shear using RheoOptica 1. A histogram of droplet size for the HPC25%/PDMS blend is shown in Fig. 4, where f_i is a normalized frequency of droplet with radius r_i. From Fig. 4, r_V and r_V/r_N are evaluated as $r_V = 14.7$ μm and $r_V/r_N = 1.93$. It was confirmed that the given $\dot{\gamma}$ is in the range where $r_V \propto \dot{\gamma}^{-1}$, or in the non-hysteresis region [22,23].

After complete breakup, the capillary number Ca ($= \eta_m \dot{\gamma} r_V/\Gamma$) for the average droplet with r_V should be smaller than the critical capillary number Ca_C for breakup. A fitting equation by de Bruijn for Ca_C data (the Grace curve) for shear flow is

$$\log Ca_C = c_0 + c_1 \log K + c_2 (\log K)^2 + \frac{c_3}{\log K - \log K_C} \tag{8}$$

with $c_0 = -0.506$, $c_1 = -0.0994$, $c_2 = 0.124$, $c_3 = -0.115$ and $K_C = 4.08$, where K_C is the critical viscosity ratio above which

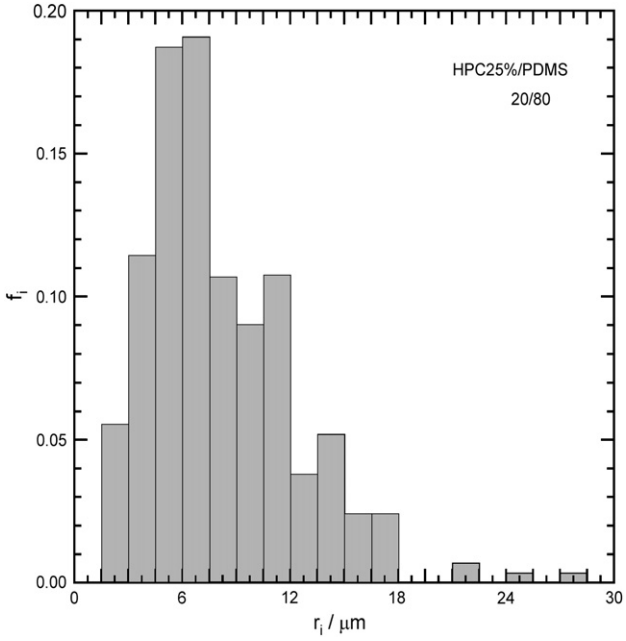

Fig. 4. Histogram for the droplet radius r_i after pre-shear of $\dot{\gamma} = 0.50\ s^{-1}$.

breakup is not possible in shear flow [23,24]. In the HPC25%/PDMS blend, $Ca_C = 0.458$ and $Ca = 0.236$, and this small Ca is consistent with the wide distribution of droplet size. The critical radius is calculated to be 28.5 μm from the Ca_C value. In Fig. 4, the cut-off of the size distribution in the HPC25%/PDMS blend is not clear, but the observed maximum radius (28 μm) is comparable with this critical radius. Concerning the size distribution in small droplets, the minimum radius observable in our optical microscope is around 1–2 μm. Smaller droplets may exist but we could not determine the smaller-size distribution. In the PIB/PDMS blend, Ca (=0.653) for the droplet with r_V is close to Ca_C (=0.701), reflecting the narrow distribution of droplet size. In a series of blends with the same Γ, the droplet size distribution is the narrowest around $K = 1$ [25]. However, smaller droplets may be stable in a blend with high Γ such as HPC25%/PDMS, resulting in the wide distribution even at $K = 0.54$.

4.3. Dynamic viscoelasticity of the 20/80 blend

First, the linear viscoelastic region was determined from the strain dependences of the storage and loss moduli, G' and G''. The amplitude of strain was set to be 0.03 for both blends and 0.2 for the components. Angular frequency dependencies of G' and G'' for the 20/80 blend of PIB/PDMS with $\phi = 0.214$ at 23 °C are shown by open circles in Fig. 5 (left and right, respectively). For a later discussion on component contribution, the frequency axis is normalized by τ_D, the relaxation time of the emulsion model of Palierne [19].

$$\tau_D = \frac{\eta_m r_V}{4\Gamma} \frac{(19K+16)[2K+3-2\phi(K-1)]}{10(K+1)-2\phi(5K+2)} \tag{9}$$

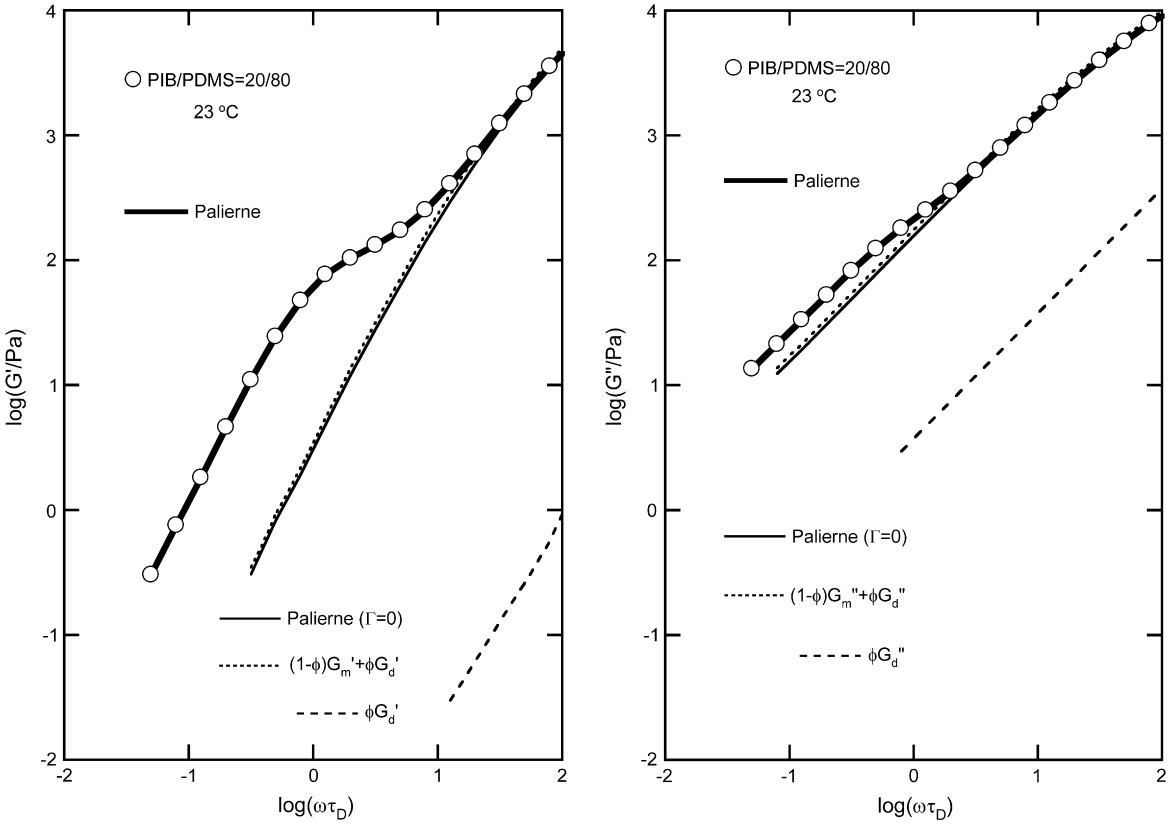

Fig. 5. Frequency dependences of the storage (left) and loss moduli (right) compared with prediction from the emulsion model ($\Gamma/r_V = 345$ Pa). Evaluated component contributions by two methods are also shown together with the minor droplet phase contribution.

A clear shoulder appears in G' due to the interface contribution in low frequency region. The thick solid lines in Fig. 5 represent prediction of the emulsion model of Palierne for G' and G''. Here, the following simplified version by Graebling *et al.* [26] is used.

$$G^*(\omega) = G^*_m(\omega)\frac{1+3\phi H(\omega)}{1-2\phi H(\omega)} \tag{10}$$

with the average viscoelastic factor $H(\omega)$ of the dispersed phase.

$$H(\omega) = \frac{(4\Gamma/r_V)\left[2G^*_m(\omega)+5G^*_d(\omega)\right]-\left[G^*_m(\omega)-G^*_d(\omega)\right]\left[16G^*_m(\omega)+19G^*_d(\omega)\right]}{(40\Gamma/r_V)\left[G^*_m(\omega)+G^*_d(\omega)\right]+\left[3G^*_m(\omega)+2G^*_d(\omega)\right]\left[16G^*_m(\omega)+19G^*_d(\omega)\right]} \tag{11}$$

In Eqs. (10) and (11), $G^*(\omega)$ is the complex modulus at ω, with subscripts m and d for matrix and dispersed phases, respectively. For various types of size distribution curves, Graebling *et al.* verified that Eqs. (10) and (11) are valid when $r_V/r_N \leq 2.0$ [26]. For the PIB/PDMS blend, agreement between the prediction and the data becomes excellent, when the value of Γ/r_V is set to be 345 Pa. The average radius $r_V = 9.0$ μm obtained from this fitting is consistent with the microscopic observation. In the HPC25%/PDMS blend, all the necessary quantities are already obtained as shown in Table 2. The Palierne prediction for $G^*(\omega)$ also agrees very well with the HPC25%/PDMS data.

Here we evaluate the component contribution to $G^*(\omega)$ in the PIB/PDMS blend in order to obtain the interface contribution. Lacroix *et al.* [27] and Vinckier and Laun [28] evaluated the component contribution by putting $\Gamma = 0$ in Eq. (11). Vinckier *et al.* verified the method by comparing the calculated modulus with experimental data in which a blend sample has the same phase-separated structure but with zero interfacial tension. This particular sample was obtained by quenching the sample below LCST [28]. Another method for evaluation of the component contribution is to adopt the linear blending rule, in which the component contribution is given by the sum of matrix and droplet contributions $[(1-\phi)G^*_m(\omega)+\phi G^*_d(\omega)]$ [28]. In Fig. 5, the component contributions evaluated by both methods are compared, where the thin solid line is obtained from the zero Γ assumption and the dotted line from the blending rule. Almost the same result for the component contribution is obtained for G' as well as for G''.

In case of G', the component contribution becomes smaller than 1/10 of the blend data at $\omega\tau_D \leq 1.7$.

4.4. Comparison between experimental and calculated excess relaxation moduli

The experimental excess modulus $\Delta G(t,\gamma)$ was evaluated from the measured relaxation moduli of the blend and the components, assuming linear additivity for the component contribution.

$$\Delta G(t,\gamma) = G(t,\gamma) - [(1-\phi)G_m(t,\gamma) + \phi G_d(t,\gamma)] \quad (12)$$

In case of miscible blends, the assumption of linear additivity is not appropriate, because a cross term is needed to describe the interactions between component polymers. However, in immiscible blends, the component polymers relax almost independently in each phase. At the instant of application of a step strain, the droplet phase deforms almost affinely in the range of $0.0476 \leq K \leq 1$. The polymer chains relax so fast while the droplet shape is flat ellipsoid. All these factors may support the application of Eq. (12). Another reason for adopting the linear blending rule is the agreement between the blending rule and the zero Γ assumption in linear viscoelasticity. In case of steady shear flow, applicability of the linear blending rule includes much more difficult problems [29,30]. In our experiments, the droplet phase component (PIB or HPC25%) relaxes very rapidly and makes a negligible contribution in each blend. The negligible droplet-phase contribution in linear viscoelasticity is already seen in Fig. 5. Thus, $\Delta G(t,\gamma)$ is evaluated by simply subtracting the matrix contribution $(1-\phi)G_m(t,\gamma)$ from the blend modulus $G(t,\gamma)$. In Fig. 6, the experimental data of $G(t,\gamma)$ and $(1-\phi)G_m(t,\gamma)$ are shown for the PIB/PDMS blend at $\gamma = 4$, together with the subtracted result, $\Delta G(t,\gamma)$, by the thick solid line. The component contribution, or $(1-\phi)G_m(t,\gamma)$ in this case, becomes smaller than 1/10 of $G(t,\gamma)$ at $t/\tau_D \geq 0.33$. Somewhat longer time ($t/\tau_D = 0.45$–0.52) was necessary for the HPC25%/PDMS blend at $\gamma = 3$ and 4 when the component contribution becomes 1/10 of $G(t,\gamma)$. In both systems, $\Delta G(t,\gamma)$ at short times (early stage of flat ellipsoid) is not reliable due to large component contributions to $G(t,\gamma)$.

In Figs. 7 and 8, the normalized modulus $(r_0/\Gamma\phi)\Delta G(t,\gamma)$ calculated for the PIB/PDMS blend at $\gamma = 3$ and 4 (solid line in each figure) is compared with experimental modulus $(r_V/\Gamma\phi)\Delta G(t,\gamma)$. Here, the normalization factor r_0/Γ for the droplet is replaced by r_V/Γ for the blend. The droplet shape in each relaxation process is specified in the figures. The dumbbell shape appears only at $\gamma \geq 4$. The calculated modulus agrees very well with $(r_V/\Gamma\phi)\Delta G(t,\gamma)$ data, even in the relaxation process with the dumbbell shape. Small deviation at long time end is due to the polydispersity of droplet radius in the real system. Comparison at short times ($t/\tau_D < 0.33$) should be semi-quantitative, due to the ambiguity in evaluation of the component contribution at very short times. Owing to the strong polydispersity effect at $\gamma = 5$, a simple comparison as given here could not be made at that strain. In Fig. 8, the stress relaxation rate after the rod-like shape accelerates while the droplet shape changes into dumbbell and finally into ellipsoid of revolution. In Figs. 7 and 8, the calculated stress with an assumption of ellipsoidal shape all through the relaxation process is represented by the dotted lines. In the dumbbell

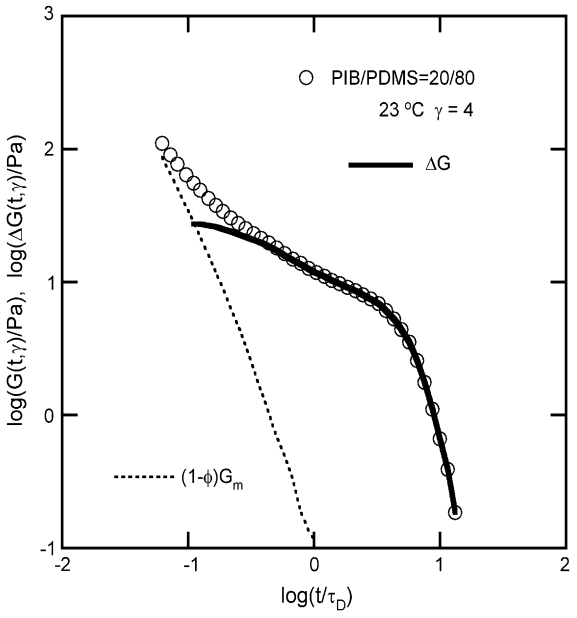

Fig. 6. Measured relaxation modulus and evaluated excess modulus for a PIB/PDMS blend at $\gamma = 4$. The matrix contribution to the relaxation modulus is also shown by the dotted line.

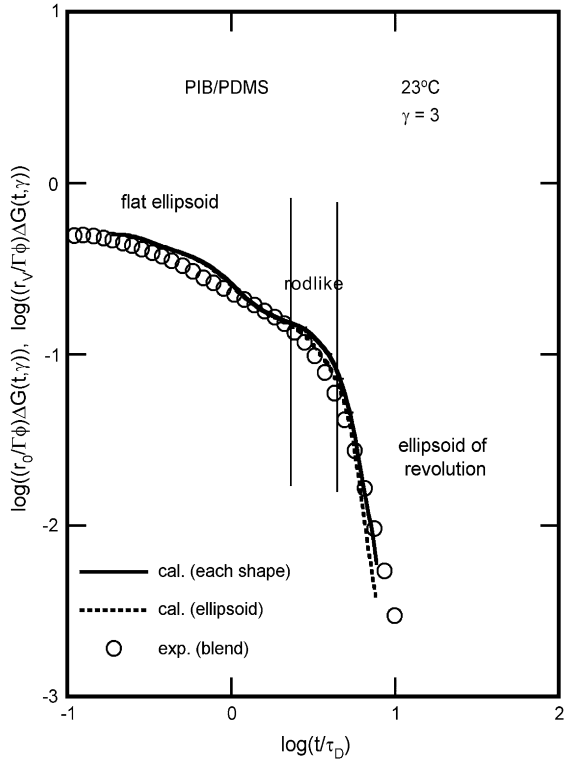

Fig. 7. Comparison between calculated and experimental time dependences of normalized excess relaxation modulus in case of narrow distribution of droplet size.

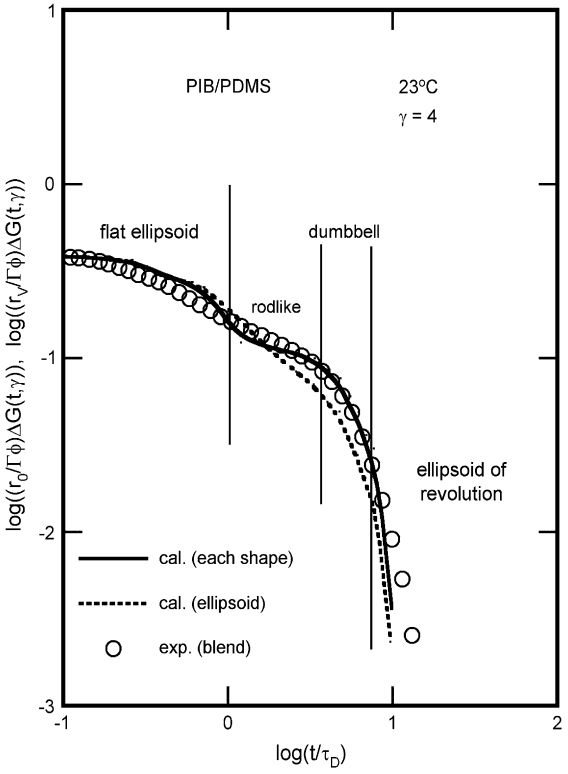

Fig. 8. Comparison similar to Fig. 7. The dumbbell shape appears at this strain.

period, the assumption of ellipsoidal shape gives lower modulus than the experimental data as shown in Fig. 8. On the other hand, the ellipsoidal assumption seems to be valid when the dumbbell shape does not appear in the process as demonstrated in Fig. 7.

Next we consider a broad distribution system like HPC25%/PDMS. Although the range of r_0 is limited (140–280 μm for PIB/PDMS and 97–252 μm for HPC25%/PDMS systems), it was revealed that the normalized semi-axes a/r_0, b/r_0 and c/r_0 become universal functions of t/τ_D and γ at given Γ, K and η_m. Here we assume that this universality can be extended to much smaller droplets. Then, we can see from Table 1 that $\Delta G(t,\gamma)$ can be written as

$$\Delta G(t,\gamma) = \frac{\Gamma\phi}{r_0} F\left(\frac{t}{\tau_D(r_0)}, \gamma\right) \tag{13}$$

by introducing a universal function F for different r_0. The contribution of ith droplet (with the radius r_i and the volume fraction ϕ_i) to $\Delta G(t,\gamma)$ becomes

$$\Delta G_i(t,\gamma) = \frac{\Gamma\phi_i}{r_i} F\left(\frac{t}{\tau_D(r_i)}, \gamma\right) \tag{14}$$

Since ith droplet contributes to $\Delta G(t,\gamma)$ independently under the condition of no breakup and no coalescence, $\Delta G(t,\gamma)$ becomes

$$\Delta G(t,\gamma) = \sum_i \Delta G_i(t,\gamma) = \Gamma \sum_i \frac{\phi_i}{r_i} F\left(\frac{t}{\tau_D(r_i)}, \gamma\right) \tag{15}$$

Then the normalized modulus is given by

$$\frac{r_V}{\Gamma\phi}\Delta G(t,\gamma) = \sum_i \frac{\phi_i}{\phi}\frac{r_V}{r_i} F\left(\frac{t}{\tau_D(r_V)\frac{r_i}{r_V}}, \gamma\right) \tag{16}$$

Eq. (16) implies that the normalized modulus can be calculated by summation of shifted F, where the horizontal and vertical shift factors are r_i/r_V and $(\phi_i/\phi)(r_V/r_i)$, respectively. The horizontal shift factor comes from the r-dependence of τ_D. From the microscopic observation of the normalized frequency f_i for droplets with r_i, ϕ_i/ϕ can be calculated by

$$\frac{\phi_i}{\phi} = \frac{f_i r_i^3}{\sum_i f_i r_i^3} \tag{17}$$

In Figs. 9 and 10, calculated and experimental normalized moduli of the HPC25%/PDMS blend are compared at $\gamma = 3$ and 5, respectively. For comparison, the calculated modulus for a single droplet approximation is represented by the broken line in each figure. It should be emphasized that the single droplet approximation fails even for a system with $r_V/r_N = 1.93$ at $\gamma \geq 3$. The effect of polydispersity becomes more prominent as γ increases, because droplets with different sizes take different shapes at long times for such large γ. Although some ambiguity still remains in evaluation of small-droplet distribution and component contribution to the modulus at short times, the proposed method for polydisperse system works reasonably well at both strains. Deviation of predicted

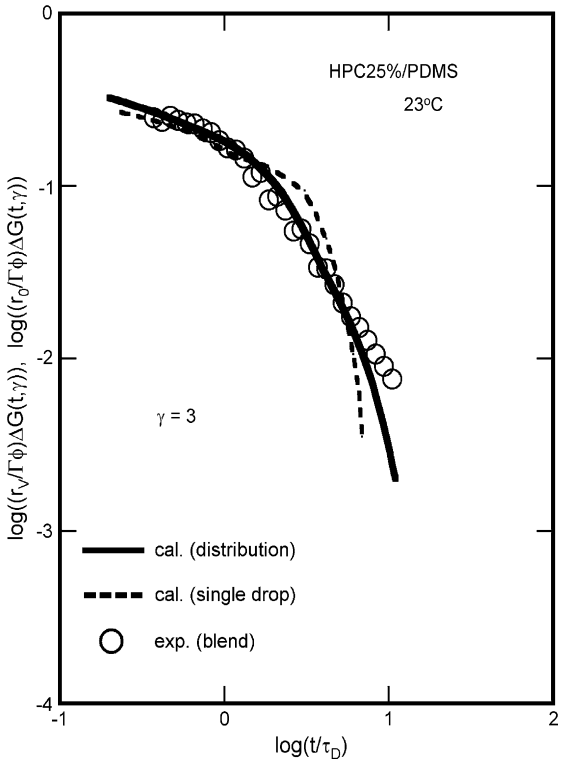

Fig. 9. Comparison of the normalized modulus in case of broad distribution of droplet size. The solid line is obtained by summation of shifted broken lines (shifted single-droplet lines) according to a proposed scaling relation.

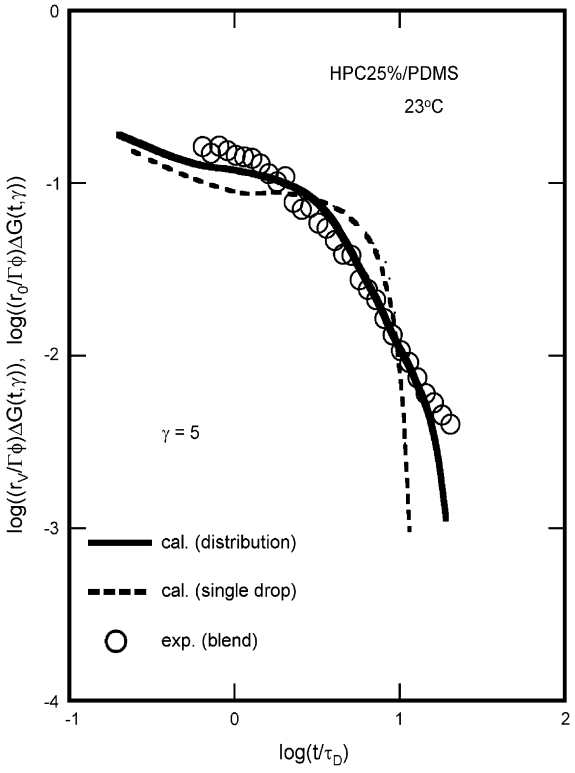

Fig. 10. Comparison similar to Fig. 9. The dumbbell shape appears at this strain.

modulus from the experimental data at long time end may be due to some ambiguity in the distribution of largest droplets. The excess relaxation modulus is predicted rather well in the present study without considering the stress term concerned with velocity at the interface and viscosity difference. It should be emphasized here that evaluation of this stress term is important in general flow field especially when the interface velocity is rather fast.

5. Conclusions

Analytical solutions (or integral equations) for the excess shear stress $\Delta\sigma_{xy}$ are obtained for droplets with the shapes of flat ellipsoid, rod with end caps, dumbbell and ellipsoid of revolution. For a 20/80 blend of PIB/PDMS with narrow distribution of droplet size ($r_V/r_N < 1.2$), predicted normalized modulus agrees very well with experimental data normalized per one droplet with the volume-averaged radius. Predicted slow relaxation in the intermediate stage with the rod-like shape and fast relaxation thereafter with the shapes of dumbbell and ellipsoid of revolution are consistent with the experimental data. The ellipsoidal assumption with the constant volume condition is valid only when the dumbbell shape does not appear in the process. For polydisperse systems, a universal function F is introduced to express simple shifts of the modulus curve with changing the droplet size r_i and its volume fraction ϕ_i. The normalized modulus is expressed by summation of shifted F, with horizontal (r_i/r_V) and vertical ($\phi_i r_V/\phi r_i$) shift factors. This method works reasonably well for a HPC/PDMS blend with broad distribution ($r_V/r_N = 1.93$).

Acknowledgments

This work was partially supported by a Grant-in-Aid for Scientific Research (B) Nos. 16350127 and 18350119 from the Japan Society for the Promotion of Science. We thank Rheo Lab Co. Ltd. and UBM Co. Ltd. in Japan for their generous help in using the rheometers Gemini (Rheo Lab) and RheoOptica 1 (UBM).

References

[1] Tucker CL, Moldenaers P. Annu Rev Fluid Mech 2002;34:177–210.
[2] Stone HA, Leal LG. J Fluid Mech 1989;198:399–427.
[3] Stone HA. Annu Rev Fluid Mech 1994;26:65–102.
[4] Batchelor GK. J Fluid Mech 1970;41:545–70.
[5] Onuki A. Phys Rev A 1987;35:5149–55.
[6] Onuki A. Europhys Lett 1994;28:175–9.
[7] Doi M, Ohta T. J Chem Phys 1991;95:1242–8.
[8] Yamane H, Takahashi M, Hayashi R, Okamoto K, Kashihara H, Masuda T. J Rheol 1998;42:567–80.
[9] Hayashi R, Takahashi M, Yamane H, Jinnai H, Watanabe H. Polymer 2001;42:757–64.
[10] Hayashi R, Takahashi M, Kajihara T, Yamane H. J Rheol 2001; 45:627–39.
[11] Okamoto K, Takahashi M, Yamane H, Kashihara H, Watanabe H, Masuda T. J Rheol 1999;43:951–65.
[12] Almusallam AS, Larson RG, Solomon MJ. J Rheol 2004;48:319–48.
[13] Maffettone PL, Greco F. J Rheol 2004;48:83–100.
[14] Yu W, Bousmina M, Zhou C, Tucker III CL. J Rheol 2004;48:417–38.
[15] Almusallam AS, Larson RG, Solomon MJ. J Rheol 2000;44:1055–83.
[16] Hayashi R, Takahashi M, Yamane H. Nihon Reoroji Gakkaishi (J Soc Rheol Jpn) 2000;28:137–42. Downloadable from http://www.jstage.jst.go.jp/browse/rheology/28/3/_contents.
[17] Okamoto K, Takahashi M, Yamane H, Watashiba H, Tsukahara Y, Masuda T. Nihon Reoroji Gakkaishi (J Soc Rheol Jpn) 1999;27:109–15. Downloadable from http://www.jstage.jst.go.jp/browse/rheology/27/2/_contents.
[18] Soskey PR, Winter HH. J Rheol 1984;28:625–45.
[19] Palierne JF. Rheol Acta 1990;29:204–14.
[20] Tomotika S. Proc Roy Soc London Ser A 1935;150:322–37.
[21] Elemans PHM, Janssen JMH, Meijer HEH. J Rheol 1990;34:1311–25.
[22] Vinckier I, Moldenaers P, Mewis J. J Rheol 1996;40:613–31.
[23] Minale M, Moldenaers P, Mewis J. Macromolecules 1997;30:5470–5.
[24] Utracki LA, Shi ZH. Polym Eng Sci 1992;32:1824–33.
[25] Kitade S, Ichikawa A, Imura N, Takahashi Y, Noda I. J Rheol 1997;41:1039–60.
[26] Graebling D, Muller R, Palierne JF. Macromolecules 1993;26:320–9.
[27] Lacroix C, Aressy M, Carreau PJ. Rheol Acta 1997;36:416–28.
[28] Vinckier I, Laun HM. J Rheol 2001;45:1373–85.
[29] Vinckier I, Moldenaers P, Mewis J. J Rheol 1997;41:705–18.
[30] Jansseune T, Moldenaers P, Mewis J. J Rheol 2003;47:829–45.